






## Research Article

# Synthesis, Characterization, and Application of Magnetized Lanthanum (III)-Based Metal-Organic Framework for the Organic Dye Removal from Water

Fatimah Mohammed Alzahrani <sup>1</sup>, Norah Salem Alsaari <sup>1</sup>,  
Khadijah Mohammedsaleh Katubi <sup>1</sup>, Abdelfattah Amari <sup>2,3</sup>  
and Mohamed A. Tahooun <sup>4,5</sup>

<sup>1</sup>Department of Chemistry, College of Science, Princess Nourah bint Abdulrahman University, P.O. Box 84428, Riyadh 11671, Saudi Arabia

<sup>2</sup>Department of Chemical Engineering, College of Engineering, King Khalid University, Abha 61411, Saudi Arabia

<sup>3</sup>Department of Chemical Engineering & Processes, Research Laboratory of Processes, Energetics, Environment and Electrical Systems, National School of Engineers, Gabes University, Gabes 6072, Tunisia

<sup>4</sup>Department of Chemistry, College of Science, King Khalid University, P.O. Box 9004, Abha 61413, Saudi Arabia

<sup>5</sup>Chemistry Department, Faculty of Science, Mansoura University, Mansoura 35516, Egypt

Correspondence should be addressed to Norah Salem Alsaari; nsalsaiari@pnu.edu.sa

Received 30 March 2022; Revised 26 April 2022; Accepted 29 June 2022; Published 18 July 2022

Academic Editor: Ibrahim H. Alsohaimi

Copyright © 2022 Fatimah Mohammed Alzahrani et al. This is an open access article distributed under the Creative Commons Attribution License, which permits unrestricted use, distribution, and reproduction in any medium, provided the original work is properly cited.

A hybrid composite based on metal-organic framework (MOF) was chemically fabricated by embedding the magnetic Fe<sub>3</sub>O<sub>4</sub> nanoparticles within amino-functionalized porous La-MOF (MOF/NH<sub>2</sub>) to produce a highly efficient and reusable composite of MOF/NH<sub>2</sub>/Fe<sub>3</sub>O<sub>4</sub>. Different proper techniques were used for the characterization of surface morphology and chemical arrangement of the prepared MOF/NH<sub>2</sub>/Fe<sub>3</sub>O<sub>4</sub> composite. The characterization results using various techniques including Fourier transform infrared spectroscopy (FT-IR), X-ray diffraction (XRD), scanning electron microscope (SEM), Brunauer, Emmett, and Teller analysis (BET), and vibrating sample magnetometer (VSM) approved the successful fabrication of MOF with amino arms on its surface besides the well magnetization using magnetic nanoparticles. The MOF/NH<sub>2</sub>/Fe<sub>3</sub>O<sub>4</sub> composite showed enhanced adsorption capacity (618 mg/g) toward methyl orange (MO) anionic dye which is higher than many commercial reported adsorbents due to the presence of many types of adsorption sites (NH<sub>2</sub> groups and lanthanum sites), large surface area of MOF, and the synergetic effect of magnetic nanoparticles. Moreover, the MOF/NH<sub>2</sub>/Fe<sub>3</sub>O<sub>4</sub> composite showed selective adsorption of MO dye from dye mixtures owing to the electrostatic attraction. Also, the MOF/NH<sub>2</sub>/Fe<sub>3</sub>O<sub>4</sub> composite retained over 90% of its efficiency for the dye removal even after six successive cycles. So, the present study provided a practical strategy for the design of functional MOF hybrid composites. Furthermore, due to the adaptability of its architectural form, it is a potential adsorbent material for industrial wastewater treatment uses.

## 1. Introduction

Water pollution due to the existence of organic dyes and toxic heavy metals is a serious problem that faces the world [1]. This problem resulted from the release of industrial wastes directly to the running water and sewage [2]. The real

danger arises from the toxic effect of these dyes and metals on the human health and living organisms [3]. Among all pollutants, organic dyes represent the most dangerous class on the environment [4]. These dyes appear in water due to the discharge of industrial wastewater including paper industries, leather industries, and textile industries. Dyes'

danger arises from its stable structure and the difficulty to biodegrade their aromatic complex structure [5]. This makes the organic dyes to be carcinogenic, mutagenic, and very toxic [6]. Subsequently, their removal from wastewater before discharge is mandatory to protect human health and other microorganisms. Great efforts have been done by scientists to achieve proper methods for dye removal from wastewater. Different methods have been accepted for the removal of organic dyes from water including ion exchange [7], membranes [8, 9], adsorption [10–19], precipitation [20], reverse osmosis [21], coagulation-flocculation [22], ozonation [23, 24], electrochemical oxidation [25], and biological treatment [26–28]. Among all methods, adsorption is the widely used method for the removal of dyes due to many factors including low cost of processing, high efficiency, fast and easy separation, no secondary pollution, and high recyclability [29, 30]. The commonly used adsorbents such as natural fibers, zeolites, and activated carbon have limited applications for the removal of organic dyes due to the poor selectivity and low adsorption capacity. So, the fabrication of new adsorbents for dye removal has become an urgent necessity. In this context, new fabricated materials such as graphene [31], carbon nanotubes [32, 33], quantum dots [34], nanocellulose [35], and metal-organic frameworks (MOFs) [36–38] have been investigated as adsorbents for water treatment. Among all adsorbents, MOFs have attracted the attention recently for the water treatment applications. MOFs are classes of fabricated inorganic-organic hybrid porous crystalline materials with magnificent properties such as high thermal stability, large surface area, large amounts of unsaturated metal sites, and tunable pore structure allowing their wide use in different fields of applications such as water treatment [39], gas separation [40], gas storage [41], sensors [42], luminescent materials [43], and drug delivery and storage [44]. In the recent decade, engineered MOFs are widely investigated for the removal of water pollutants. Because metal ion is frequently used as an active site for a variety of applications, choosing the right metal ion for the framework is always critical. Lanthanide-based metals are excellent choice for the fabrication of MOFs due to their high valence state (normally +3) giving high complexation mode and flexibility giving architectural diversity into the MOFs [45]. All these advantages of MOFs make them appropriate applicant for adsorption of different pollutants from water.

However, MOFs as adsorbents have limitations due to the difficulty of separation from adsorption environment as their separation requires filtration and high-speed centrifugation. This makes the magnetization of the MOFs essential for their application as adsorbents for water treatment to ease their separation using an external magnet. Magnetic nanoparticles are favored because they have various advantages, including a wide surface area, low toxicity, low cost, environmental friendliness, and reusability, in addition to being collected by an external magnet and not requiring centrifugation. The dispersibility and magnetism loss are the essential disadvantage of magnetic nanoparticles that result from its tendency to oxidation. Magnetic nanoparticles are usually coated and treated with different materials to pro-

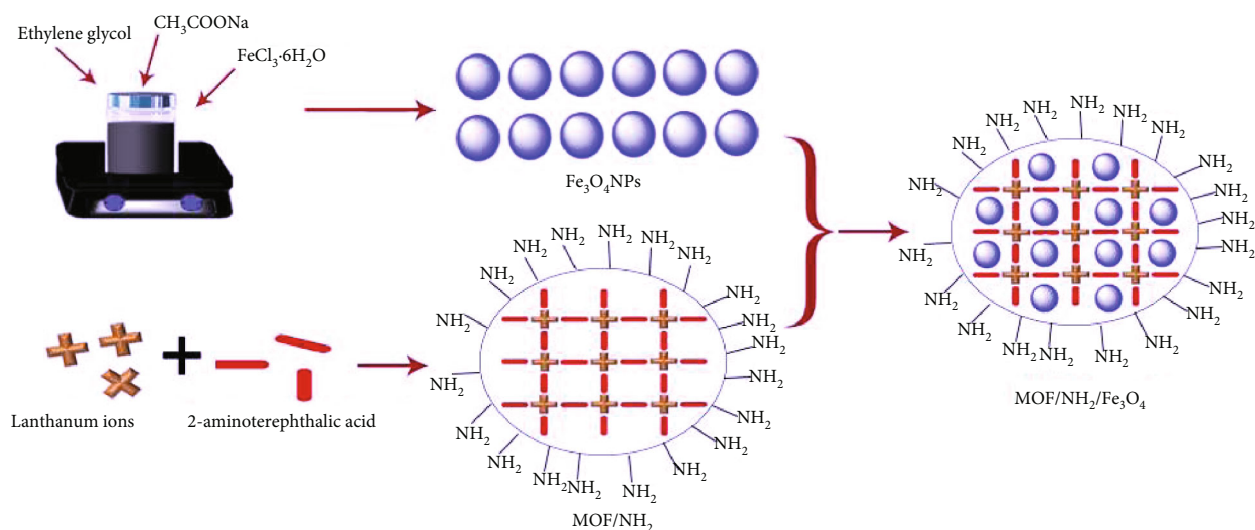
vide stability and prevent aggregation. The hybrid magnetic adsorbents have advantages over magnetic nanoparticles, like providing active sites for effective capturing of pollutants and enhance the selectivity and adsorption ability. Subsequently, the association of MOF blocks with magnetic nanoparticles will enhance the capacity of the hybrid during treatment process with solving the issues of adsorbent separation from the medium after adsorption process. This magnetic separation provides the ability for using the adsorbent several times for water treatment. This makes the magnetic MOFs as adsorbent cost-effective from the economical view. In the present study, all these features are taken into account during the fabrication of the adsorbent to enhance its large-scale (industrial) application.

Herein, a nanosized, highly efficient, and recyclable adsorbent based on La-MOFs was synthesized. The La-MOFs were amino-functionalized to produce La-MOFs-NH<sub>2</sub> to allow the surface modification of the La-MOFs using the magnetic Fe<sub>3</sub>O<sub>4</sub> nanoparticles and fabricate a composite, namely, La-MOFs/NH<sub>2</sub>/Fe<sub>3</sub>O<sub>4</sub>. The synthesized nanomaterials were characterized using proper techniques including scanning electron microscopy (SEM), Fourier transform infrared spectroscopy (FT-IR), X-ray diffraction (XRD), thermogravimetric analysis (TGA), and Brunauer-Emmett-Teller (BET). The synthesized composite was examined for the removal of methyl orange (MO) as a model dye. Moreover, the adsorption kinetics and adsorption isotherm for MO uptake on the surface of MOFs/NH<sub>2</sub>/Fe<sub>3</sub>O<sub>4</sub> composite were studied. Also, the reusability of the MOFs/NH<sub>2</sub>/Fe<sub>3</sub>O<sub>4</sub> composite as adsorbent was determined for MO removal for up to five cycles. Finally, the efficiency of MOFs/NH<sub>2</sub>/Fe<sub>3</sub>O<sub>4</sub> composite as adsorbent for dye removal was evaluated. The originality and novelty of the present study are based on the following criteria: (1) the magnetization of La-based MOF to enhance its adsorption capacity and reusability toward the adsorption of organic dyes; (2) to the best of our knowledge, there is no information about the capacity of the synthesized composite toward MO dye removal; (3) information on the removal of MO dye will be added to the current literature as a result of this study.

## 2. Experimental

**2.1. Chemicals.** Methyl orange (MO) was purchased from Aladdin Co. *N,N*-Dimethylformamide (DMF), hydrochloric acid, and sodium acetate were purchased from El-Gomhouria Co., Egypt. Ethylene glycol, ferric chloride hexahydrate, lanthanum nitrate hexahydrate, and 2-aminoterephthalic acid were purchased from Sigma-Aldrich. All chemicals were used as received without any further purification. Deionized water was used for the preparation of all solutions.

**2.2. Synthesis of Magnetic Nanoparticles.** The magnetic Fe<sub>3</sub>O<sub>4</sub> nanoparticles were synthesized using solvothermal method as described in the literature [46]. Typically, a colloidal solution was prepared at room temperature under strong stirring by dissolving 8.2 g of sodium acetate and 2.7 g of ferric chloride hexahydrate in 60.0 mL of ethylene glycol. The stirring process was continued for half-hour then poured



SCHEME 1: The schematic diagram for the synthesis of MOFs/NH<sub>2</sub>/Fe<sub>3</sub>O<sub>4</sub> composite.

into stainless steel autoclave and heated for 10.0 hours at 200°C. After that, the mixture was kept to cool down in room temperature and the formed magnetic Fe<sub>3</sub>O<sub>4</sub> nanoparticles were collected using a magnet. The collected magnetic nanoparticles were washed several times using deionized H<sub>2</sub>O and methanol. Finally, the Fe<sub>3</sub>O<sub>4</sub> nanoparticles are dried in the oven for 10.0 hours at 65°C.

**2.3. Synthesis of Amino-Functionalized La-MOFs.** The synthesis of amino-functionalized La-MOFs (MOFs/NH<sub>2</sub>) was synthesized as described in the literature [47]. Typically at room temperature, 30 mL of DMF solvent was used to dissolve 0.363 g of 2-aminoterephthalic acid and 0.886 g of lanthanum nitrate hexahydrate with continuous stirring for 15 minutes. Then, the solution was poured into stainless steel autoclave and heated for 6.0 hours at 150°C. After that, the solution was kept to cool down at room temperature and the obtained MOFs/NH<sub>2</sub> was washed several times with deionized H<sub>2</sub>O and methanol. Finally, the MOFs/NH<sub>2</sub> was dried for 1 day at 65°C in vacuum.

**2.4. Synthesis of MOFs/NH<sub>2</sub>/Fe<sub>3</sub>O<sub>4</sub> Composite.** Firstly, 30 mL of DMF solvent was used to dissolve 0.363 g of 2-aminoterephthalic acid and 0.886 g of lanthanum nitrate hexahydrate. Then, 10 mL of DMF solution was used to dissolve 0.115 g of magnetic Fe<sub>3</sub>O<sub>4</sub> nanoparticles under ultrasonication to prevent the nanoparticles' aggregation. After that, the magnetic Fe<sub>3</sub>O<sub>4</sub> nanoparticles solution was added to the firstly prepared solution with stirring for half-hours. The mixture was then poured into a stainless steel autoclave and heated for 6.0 hours at 150°C. The obtained solution was kept to cool down at room temperature and the formed MOFs/NH<sub>2</sub>/Fe<sub>3</sub>O<sub>4</sub> composite was collected using an external magnet and washed several times using methanol and deionized H<sub>2</sub>O. Finally, the formed composite was dried for 1 day at 65°C. Scheme 1 illustrates the synthesis method of the MOFs/NH<sub>2</sub>/Fe<sub>3</sub>O<sub>4</sub> composite.

**2.5. Batch Adsorption Study.** The adsorption performance of the synthesized MOFs/NH<sub>2</sub>/Fe<sub>3</sub>O<sub>4</sub> composite was evaluated using MO dye as a model at different experimental conditions. All experiments were performed at 25°C. The adsorption conditions were optimized by studying the effect of different parameters including pH, contact time, initial dye concentration, and adsorbent dose. In each experiment, a certain amount of adsorbent is shaken with 80 mL of dye solution of a certain concentration at 200 rpm. After that, the adsorbent was collected using an external magnet and the solution was examined for the presence of MO dye using UV-Visible spectrophotometer at  $\lambda = 465$  nm. During the study of pH effect, the pH values were adjusted using 0.1 M of KOH and HCl solutions. The adsorption isotherm study was performed using initial concentration ranging from 50 ppm to 700 ppm. The adsorption kinetics was performed using initial concentration of 400 ppm at different contact times. The adsorption capacities were calculated according to Eq.(1).

$$q_e = \left( C_0 - \frac{C_e}{m} \right) V, \quad (1)$$

where  $q_e$ ,  $C_0$ ,  $C_e$ ,  $m$ , and  $V$  denote the adsorption capacity at equilibrium, the initial dye concentration, the dye concentration at equilibrium, the mass of adsorbent, and the volume of solution, respectively.

The removal efficiency (%) was calculated according to Eq.(2).

$$\text{Removal efficiency (\%)} = \left( C_0 - \frac{C_e}{C_0} \right) 100. \quad (2)$$

Moreover, the reusability of MOFs/NH<sub>2</sub>/Fe<sub>3</sub>O<sub>4</sub> composite as adsorbent was studied for up to five successive cycles. During the adsorption-desorption, the adsorbent was used to adsorb the dye followed by desorption of the dye from

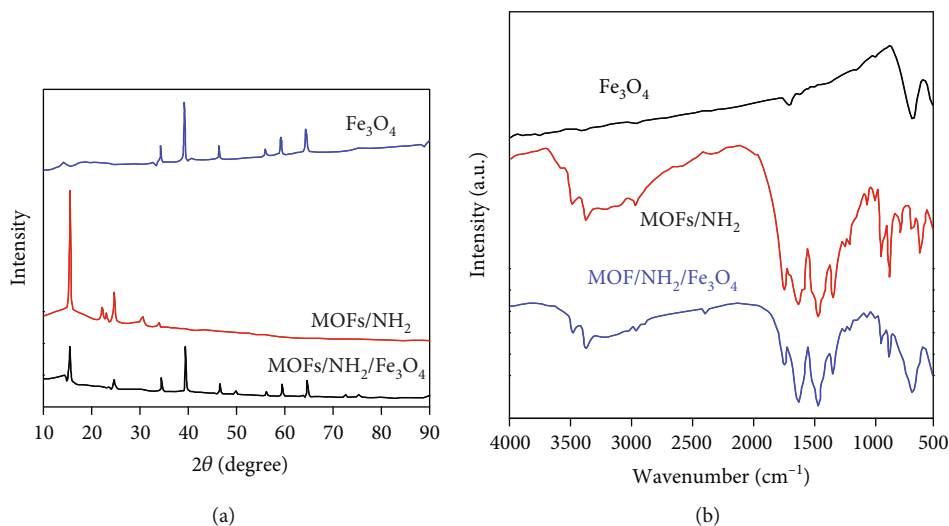


FIGURE 1: XRD (a) and FT-IR (b) of the synthesized  $\text{Fe}_3\text{O}_4$  nanoparticles,  $\text{MOF}/\text{NH}_2$ , and  $\text{MOF}/\text{NH}_2/\text{Fe}_3\text{O}_4$ .

the surface of the adsorbent using methanol. Then, the adsorbent was used for another cycle. After each adsorption experiment, the adsorbent was collected using an external magnet. Finally, depending on the removal efficiencies, the reusability of the adsorbent was evaluated.

### 3. Results and Discussion

**3.1. The Characterization of Materials.** The characterization of synthesized materials was achieved using familiar techniques. For the determination of the present functional groups, FT-IR spectra for the synthesized  $\text{MOF}/\text{NH}_2/\text{Fe}_3\text{O}_4$ ,  $\text{MOF}/\text{NH}_2$ , and magnetic  $\text{Fe}_3\text{O}_4$  nanoparticles were performed in the range of 4000 to 400  $\text{cm}^{-1}$  as shown in Figure 1(a). According to Figure 1(a), the FT-IR spectrum of magnetic nanoparticles showed the appearance of a broad strong band of Fe-O at 584  $\text{cm}^{-1}$  [48]. This characteristic band of magnetic nanoparticles was also observed in the spectrum of  $\text{MOF}/\text{NH}_2/\text{Fe}_3\text{O}_4$  which indicated the successful embedding of magnetic nanoparticles within the synthesized composite. Moreover, the  $\text{MOF}/\text{NH}_2/\text{Fe}_3\text{O}_4$  and  $\text{MOF}/\text{NH}_2$  spectra showed the appearance of absorption bands at 3475  $\text{cm}^{-1}$ , 3354  $\text{cm}^{-1}$ , and 1546  $\text{cm}^{-1}$  which are corresponding to the bending and stretching vibration of the  $\text{NH}_2$  group [49].

For the determination of the phase structure of synthesized materials, XRD patterns of  $\text{MOF}/\text{NH}_2/\text{Fe}_3\text{O}_4$ ,  $\text{MOF}/\text{NH}_2$ , and magnetic  $\text{Fe}_3\text{O}_4$  nanoparticles were performed in the range of  $2\theta = 5$  to  $80^\circ$  as shown in Figure 1(b). According to Figure 1(b), the XRD of magnetic nanoparticles indicated the cubic phase of magnetic nanoparticles due to the appearance of planes (440), (511), (422), (400), (311), and (220) at 62.6°, 57.0°, 39.7°, 43.0°, 35.3°, and 30.0°, respectively [50]. The size of magnetic nanoparticles was determined using the Scherrer equation and their size was found to be equal to 47 nm. Additionally, the XRD of  $\text{MOF}/\text{NH}_2$  showed the appearance of characteristic diffraction peaks at 19.8°, 17.0°, and 10.0° [47]. We can understand from the XRD of  $\text{MOF}/\text{NH}_2/\text{Fe}_3\text{O}_4$  composite that the appearance of mag-

netic nanoparticles peaks beside the peaks of  $\text{MOF}/\text{NH}_2$ , the successful combination between the magnetic nanoparticles and  $\text{MOF}/\text{NH}_2$ . Also, the reduction of peak intensity indicated the interaction between the  $\text{Fe}_3\text{O}_4$  nanoparticles and  $\text{MOF}/\text{NH}_2$ . The XRD results confirmed the FT-IR results for the successful fabrication of the target composite.

For the characterization of size and morphology, the SEM analysis was performed for the synthesized  $\text{Fe}_3\text{O}_4$  nanoparticles,  $\text{MOF}/\text{NH}_2$ , and  $\text{MOF}/\text{NH}_2/\text{Fe}_3\text{O}_4$  composite as shown in Figure 2. Figure 2(a) illustrates the SEM image of  $\text{Fe}_3\text{O}_4$  nanoparticles that clearly appears to have round biscuit-like morphology with nanoscaled size. Moreover, Figure 2(b) shows the SEM image of amino-functionalized MOFs ( $\text{MOF}/\text{NH}_2$ ) that appear to have wool ball-like morphology. Figure 2(c) shows the SEM image of  $\text{MOF}/\text{NH}_2/\text{Fe}_3\text{O}_4$  microstructured composite that clearly shows the excellent coating of magnetic nanoparticles on the surface of  $\text{MOF}/\text{NH}_2$  to correctly fabricate the composite. Subsequently, the SEM results are in agreement with XRD and FT-IR results confirming the successful loading of magnetic  $\text{Fe}_3\text{O}_4$  nanoparticles on the surface of  $\text{MOF}/\text{NH}_2$ .

To study the thermal stability of the synthesized materials, TGA curves are shown in Figure 3(a). According to Figure 3(a),  $\text{Fe}_3\text{O}_4$  nanoparticles showed the highest thermal stability, while  $\text{MOF}/\text{NH}_2$  showed a similar trend with lower thermal stability than  $\text{MOF}/\text{NH}_2/\text{Fe}_3\text{O}_4$  which was attributed to the addition of magnetic  $\text{Fe}_3\text{O}_4$  nanoparticles.  $\text{MOF}/\text{NH}_2/\text{Fe}_3\text{O}_4$  composite showed gradual weight loss within two stages. The first stage occurred in the temperature range of 30°C to 400°C with a weight loss of 19% and attributed to the evaporation of adsorbed solvent molecules. The second stage occurred in the temperature range of 400°C to 700°C with a weight loss of 21% and attributed to the decay of organic linkers and decomposition of MOF. The thermal stability results according to Figure 3(a) revealed the good stability of the synthesized materials. Moreover, the differences in TGA results indicated the successful construction of the  $\text{MOF}/\text{NH}_2/\text{Fe}_3\text{O}_4$  composite.

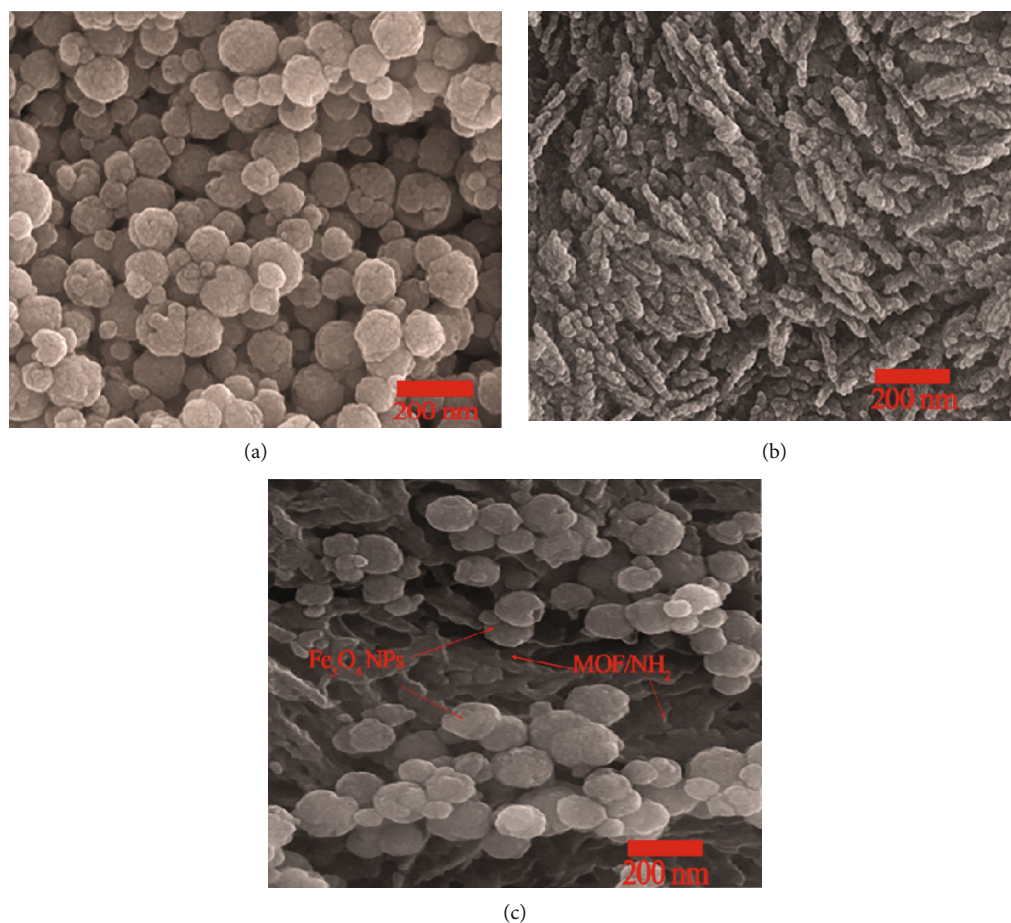


FIGURE 2: SEM images of Fe<sub>3</sub>O<sub>4</sub> nanoparticles (a), MOF/NH<sub>2</sub> (b), and MOF/NH<sub>2</sub>/Fe<sub>3</sub>O<sub>4</sub> composite (c).

One of the advantages of magnetic adsorbents is the magnetic separation that allows the ease and simple separation from the adsorption medium. Subsequently, the magnetic behavior of the synthesized Fe<sub>3</sub>O<sub>4</sub> nanoparticles and MOF/NH<sub>2</sub>/Fe<sub>3</sub>O<sub>4</sub> composite was studied using VSM as shown in Figure 3(b). According to Figure 3(b), the MOF/NH<sub>2</sub>/Fe<sub>3</sub>O<sub>4</sub> composite showed a lower saturation magnetization (16 emu g<sup>-1</sup>) than Fe<sub>3</sub>O<sub>4</sub> nanoparticles (89.34 emu g<sup>-1</sup>). This is attributed to the addition of nonmagnetic MOF/NH<sub>2</sub> to the magnetic Fe<sub>3</sub>O<sub>4</sub> nanoparticles that caused the drop in the saturation magnetization. So, the paramagnetic behavior of the synthesized MOF/NH<sub>2</sub>/Fe<sub>3</sub>O<sub>4</sub> composite allows their simple separation using an external magnetic field and enables their reusability several times for water treatment that in turn reduces the overall cost of the treatment.

Furthermore, N<sub>2</sub> adsorption-desorption isotherm results of the synthesized materials were used for the characterization of geometrical properties as shown in Figure 3(c). These properties include pore volume, average pore diameter, and specific surface area ( $S_{\text{BET}}$ ). According to Figure 3(c), the MOF/NH<sub>2</sub>/Fe<sub>3</sub>O<sub>4</sub> composite (36.2 m<sup>2</sup> g<sup>-1</sup>) showed a higher  $S_{\text{BET}}$  than MOF/NH<sub>2</sub> (32.11 m<sup>2</sup> g<sup>-1</sup>) due to the addition of magnetic Fe<sub>3</sub>O<sub>4</sub> nanoparticles. Additionally, the MOF/NH<sub>2</sub>/Fe<sub>3</sub>O<sub>4</sub> composite and MOF/NH<sub>2</sub> showed average pore diameters of 16.35 nm and 16.21 nm (BJH method), respec-

tively, with mesoporous structure. This average pore diameter is appropriate enough for entrapping the dye molecules within their building. So, the addition of magnetic Fe<sub>3</sub>O<sub>4</sub> nanoparticles to MOF/NH<sub>2</sub> provides more spaces and active sites to dye uptake and enhances the adsorption capacity.

**3.2. Factors Affecting the Adsorption Capacity.** For the optimization of adsorption conditions, the effect of different parameters (initial MO concentration, contact time, and pH value) on the dye adsorption on the surface of Fe<sub>3</sub>O<sub>4</sub> nanoparticles and MOF/NH<sub>2</sub>/Fe<sub>3</sub>O<sub>4</sub> composite was studied as shown in Figure 4. Figure 4(a) shows the plot of initial MO concentration against the adsorption capacity of Fe<sub>3</sub>O<sub>4</sub> nanoparticles and MOF/NH<sub>2</sub>/Fe<sub>3</sub>O<sub>4</sub> composite. According to Figure 4(a), the increased initial dye concentration from 0 to 400 ppm showed an increase in the adsorption capacity due to the availability of large number of adsorption sites on the surface of the Fe<sub>3</sub>O<sub>4</sub> nanoparticles and MOF/NH<sub>2</sub>/Fe<sub>3</sub>O<sub>4</sub> composite. After 400 ppm, the adsorption capacities of Fe<sub>3</sub>O<sub>4</sub> nanoparticles and MOF/NH<sub>2</sub>/Fe<sub>3</sub>O<sub>4</sub> composite were almost constant due to the increased number of dye molecules with regard to the adsorption sites (saturation process). So, 400 ppm is considered the optimum initial concentration at which the adsorption process reached its equilibrium. Also, there is a significant difference in the adsorption capacity between Fe<sub>3</sub>O<sub>4</sub> nanoparticles (124 mg/g) and MOF/NH<sub>2</sub>/

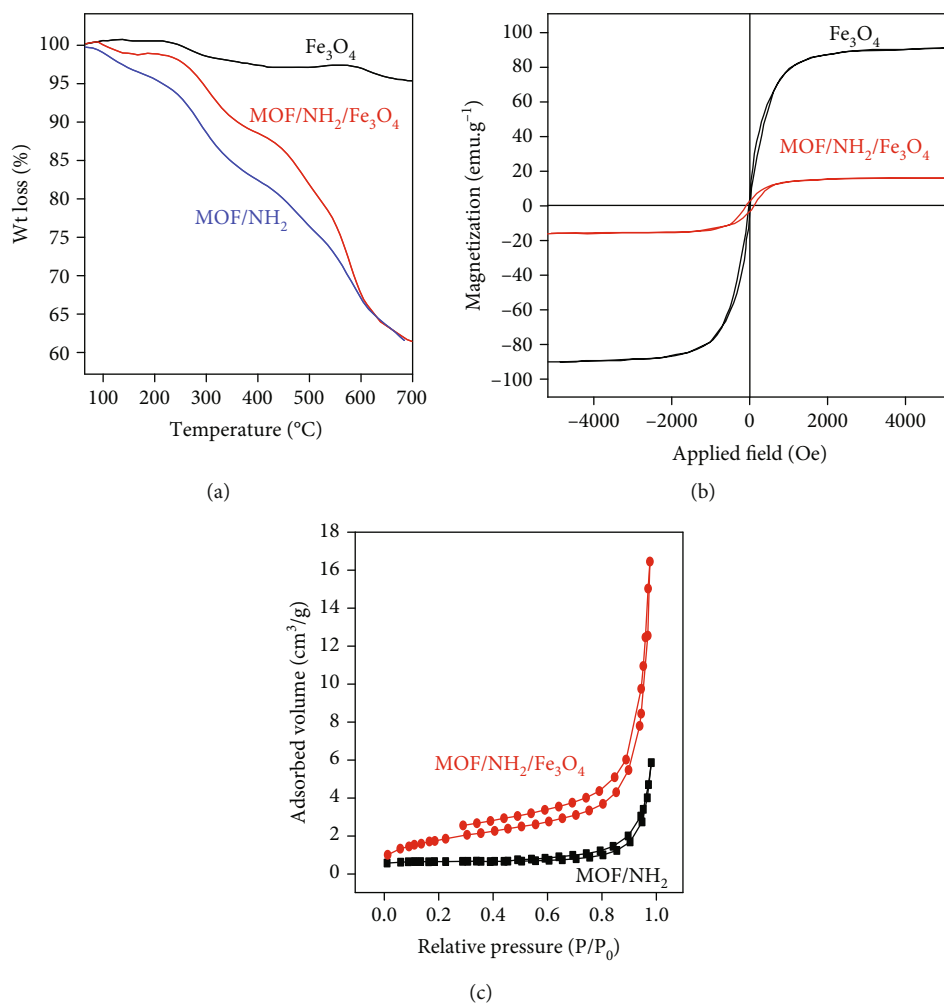


FIGURE 3: TGA curve (a), magnetization curve (b), and N<sub>2</sub> adsorption-desorption isotherms (c) of the synthesized Fe<sub>3</sub>O<sub>4</sub> nanoparticles, MOF/NH<sub>2</sub>, and MOF/NH<sub>2</sub>/Fe<sub>3</sub>O<sub>4</sub>.

Fe<sub>3</sub>O<sub>4</sub> composite (618 mg/g) indicating the enhanced adsorption capacity resulted from the magnetization of MOF crystals. This enhanced capacity is attributed to the highly porous construction of MOF/NH<sub>2</sub>/Fe<sub>3</sub>O<sub>4</sub> besides the large surface area of MOF that speeds the mass transfer for quick dye uptake [51]. Another important factor affecting the adsorption process is the contact time. Subsequently, the adsorption capacity of Fe<sub>3</sub>O<sub>4</sub> nanoparticles and MOF/NH<sub>2</sub>/Fe<sub>3</sub>O<sub>4</sub> composite for MO adsorption was studied in the range of 0 to 250 min as shown in Figure 4(b). According to Figure 4(b), the increased contact time caused an increase in the adsorption capacities of Fe<sub>3</sub>O<sub>4</sub> nanoparticles and MOF/NH<sub>2</sub>/Fe<sub>3</sub>O<sub>4</sub> composite until it reaches the equilibrium at 180 min and 60 min, respectively. After that time, the adsorption capacity almost remains constant. This behavior is attributed to the availability of large numbers of active sites for the dye uptake in the first stage, while the second stage in which the equilibrium was reached represents the saturation of all active sites with MO dye. Also, there is a significant difference between optimum contact time for Fe<sub>3</sub>O<sub>4</sub> nanoparticles and MOF/NH<sub>2</sub>/Fe<sub>3</sub>O<sub>4</sub> composite reflecting the role of MOF in driving the adsorption process.

Moreover, pH as a significant factor greatly affecting the adsorption process was studied in the range of 4 to 10 as shown in Figure 4(c) for the adsorption of MO on the surface of Fe<sub>3</sub>O<sub>4</sub> nanoparticles and MOF/NH<sub>2</sub>/Fe<sub>3</sub>O<sub>4</sub> composite. According to Figure 4(c), the adsorption capacity for Fe<sub>3</sub>O<sub>4</sub> nanoparticles showed a decrease with the increased pH values from 4 to 10. This behavior could be attributed to the -ve charge on the nanoparticle surface that increased with pH increase that causes an electrostatic repulsion between nanoparticles and anionic dye. But, pH value has a great effect on the adsorption capacity of MOF/NH<sub>2</sub>/Fe<sub>3</sub>O<sub>4</sub> composite. The adsorption capacity of MOF/NH<sub>2</sub>/Fe<sub>3</sub>O<sub>4</sub> composite toward MO dye was increased by increasing pH value from 4 to 6 due to the protonation of functional groups (+ve) on the surface of composite that induces the electrostatic attraction between adsorbent and anionic MO dye (as shown in Zeta potential results in Figure 4(d)), while at pH > 6, the adsorption capacity of the MOF/NH<sub>2</sub>/Fe<sub>3</sub>O<sub>4</sub> composite was decreased with the any increase in the pH value. This behavior is attributed to the repulsion between the anionic dye and the negatively charged adsorbent at high pH values. Additionally, the decreased adsorption capacity of MOF/NH<sub>2</sub>/Fe<sub>3</sub>O<sub>4</sub> composite

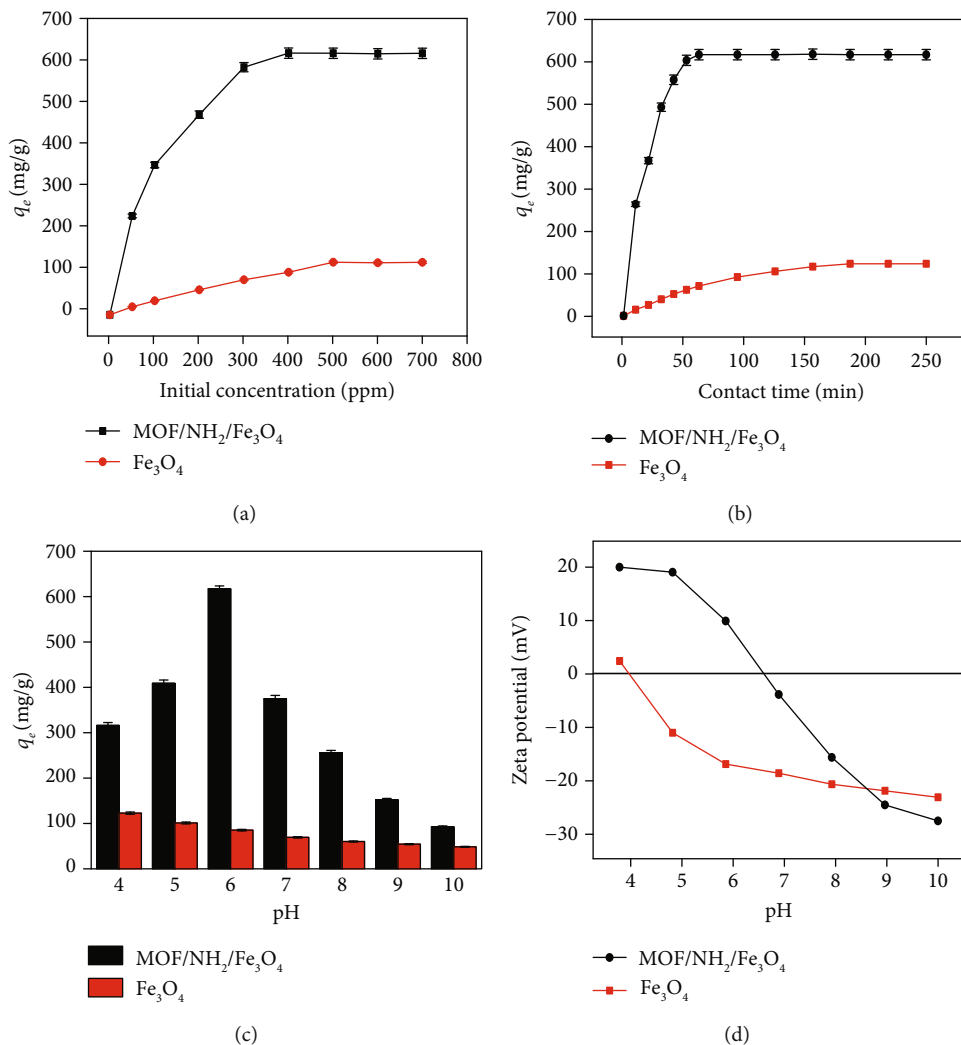


FIGURE 4: The effect of initial dye concentration (a), effect of contact time (b), effect of pH (c), and Zeta potentials (d) for the adsorption of MO on the surface of  $\text{Fe}_3\text{O}_4$  nanoparticles and  $\text{MOF}/\text{NH}_2/\text{Fe}_3\text{O}_4$ .

at high pH values may be attributed also to the repulsion between the anionic MO dye and excess  $\text{OH}^-$  groups in the solution. So, pH has complicated effect on the adsorption of pollutants on the surface of  $\text{MOF}/\text{NH}_2/\text{Fe}_3\text{O}_4$  composite.

**3.3. Adsorption Isotherm and Kinetics.** To understand the adsorption of MO dye on the surface of  $\text{MOF}/\text{NH}_2/\text{Fe}_3\text{O}_4$  composite, it is important to study the isotherm and kinetic models [52, 53]. Herein, the Langmuir and Freundlich isotherm models were used to fit the adsorption data of MO dye on the surface of  $\text{MOF}/\text{NH}_2/\text{Fe}_3\text{O}_4$  composite and  $\text{Fe}_3\text{O}_4$  nanoparticles. The Langmuir and Freundlich isotherm models can be represented according to Eq.(3) and Eq.(4), respectively [54, 55].

$$\frac{C_e}{q_e} = \frac{1}{q_m K_L} + \frac{C_e}{q_m}, \quad (3)$$

$$\ln q_e = \frac{1}{n} \ln C_e + \ln K_F, \quad (4)$$

where  $K_L$ ,  $q_m$ ,  $K_F$ , and  $n$  refer to the Langmuir constant, maximum monolayer adsorption capacity, the Freundlich constant of adsorption capacity, and the Freundlich constant of adsorption intensity, respectively. Langmuir and Freundlich's parameters are presented in Table 1.

The Langmuir model suggests that the adsorption active sites on the surface of adsorbent are energetically identical and therefore capturing the adsorbate molecules as a monolayer over the homogenous surface of adsorbent [56, 57], while the Freundlich model suggests that the adsorption active sites on the surface of adsorbent are not the same energetically and therefore capturing the adsorbate molecules as multilayers over the heterogeneous surface of adsorbent [58, 59]. The fitting of experimental data for the adsorption of MO dye on the surface of  $\text{MOF}/\text{NH}_2/\text{Fe}_3\text{O}_4$  composite and  $\text{Fe}_3\text{O}_4$  nanoparticles with the Langmuir and Freundlich models are presented in Figures 5(a) and 5(b). Regression coefficient ( $R^2$ ) value indicates the most suitable model to describe the experimental data. According to Table 1, the Langmuir model

TABLE 1: The isotherm and kinetics parameters for the adsorption of MO dye on the surface of  $\text{Fe}_3\text{O}_4$  nanoparticles and MOF/ $\text{NH}_2/\text{Fe}_3\text{O}_4$  composite.

Item	Coefficient	Adsorbent	
		$\text{Fe}_3\text{O}_4$	MOF/ $\text{NH}_2/\text{Fe}_3\text{O}_4$
Langmuir isotherm	$R^2$	0.998	0.999
	$K_L$	0.002	0.008
	$q_m$ (mg/g)	123.9	618.0
Freundlich isotherm	$R^2$	0.993	0.994
	$n$	1.219	2.118
	$K_F$	1.396	38.29
Pseudo 1 <sup>st</sup> order	$R^2$	0.969	0.948
	$K_1$	0.019	0.079
	$q_e$ (mg/g)	150.75	1030.5
Pseudo 2 <sup>nd</sup> order	$R^2$	0.988	0.983
	$K_2$	$2.63 \times 10^{-5}$	$4.10 \times 10^{-5}$
	$q_e$ (mg/g)	244.0	909.0

has higher  $R^2$  value than the Freundlich model for the adsorption of MO dye on the surface of both MOF/ $\text{NH}_2/\text{Fe}_3\text{O}_4$  composite and  $\text{Fe}_3\text{O}_4$  nanoparticles. This indicates that the Langmuir isotherm model is more suitable to describe the adsorption of MO dye on the surface of MOF/ $\text{NH}_2/\text{Fe}_3\text{O}_4$  and  $\text{Fe}_3\text{O}_4$  adsorbents. This means that the adsorption of MO dye on MOF/ $\text{NH}_2/\text{Fe}_3\text{O}_4$  and  $\text{Fe}_3\text{O}_4$  was achieved as monolayer uptake on the homogenous surface of adsorbent. However,  $R^2$  values for the Freundlich isotherm model are still acceptable value indicating that the adsorption of MO dye on the used adsorbents not occurred completely as homogenous monolayer. Additionally, the Freundlich constant ( $n$ ) that represents the strength of adsorption is higher for MOF/ $\text{NH}_2/\text{Fe}_3\text{O}_4$  than  $\text{Fe}_3\text{O}_4$  indicating that the MOF/ $\text{NH}_2/\text{Fe}_3\text{O}_4$  composite has better affinity toward the dye than the magnetic  $\text{Fe}_3\text{O}_4$  nanoparticles. This high affinity between the MO dye and MOF/ $\text{NH}_2/\text{Fe}_3\text{O}_4$  resulted from the strong electrostatic attraction between the negative charge on the dye molecule and the positive charge provided by La(III) in the MOF that has major effect in the uptake mechanism.

For more understanding of the adsorption mechanism and speed, the adsorption data were analyzed using kinetic models. So, the experimental adsorption data for the removal of MO dye on the surface of MOF/ $\text{NH}_2/\text{Fe}_3\text{O}_4$  composite and  $\text{Fe}_3\text{O}_4$  nanoparticles were fitted using the well-known kinetic models, pseudo 1<sup>st</sup> order model and pseudo 2<sup>nd</sup> order model as shown in Figures 5(c) and 5(d). The pseudo 1<sup>st</sup> order and pseudo 2<sup>nd</sup> order models can be expressed according to Eq.(5) and Eq.(6), respectively [60, 61].

$$\ln(q_e - q_t) = \ln q_e - k_1 t, \quad (5)$$

$$\frac{t}{q_t} = \frac{1}{k_2 q_e^2} + \frac{t}{q_e}, \quad (6)$$

where  $k_1$  and  $k_2$  refer to the pseudo 1<sup>st</sup> order and pseudo 2<sup>nd</sup> order rate constants with the units ( $\text{min}^{-1}$ ) and ( $\text{g mg}^{-1} \text{min}^{-1}$ ), respectively. The pseudo 1<sup>st</sup> order and pseudo 2<sup>nd</sup> order constants are presented in Table 1.

The pseudo 1<sup>st</sup> order model suggested that the adsorption of adsorbate ions was achieved on the adsorbent surface via physisorption mechanism and subsequently depending on the number of the vacant active sites [62]. But, the pseudo 2<sup>nd</sup> order model suggested that the adsorption of adsorbate ions was achieved on the adsorbent surface via chemisorption mechanism through exchange or sharing the electrons [63]. Like the isotherm study, the regression coefficient ( $R^2$ ) value indicates the most suitable model to describe the experimental data. According to Table 1, the  $R^2$  value is higher for the pseudo 2<sup>nd</sup> order than the pseudo 1<sup>st</sup> order for the adsorption of MO dye on the surface of MOF/ $\text{NH}_2/\text{Fe}_3\text{O}_4$  composite and  $\text{Fe}_3\text{O}_4$  nanoparticles. This indicates that the removals of MO dye on the surface of MOF/ $\text{NH}_2/\text{Fe}_3\text{O}_4$  composite and  $\text{Fe}_3\text{O}_4$  nanoparticles were achieved via a chemisorption mechanism. Additionally, the practical  $q_e$  value was much closer to the calculated  $q_e$  value of the pseudo 2<sup>nd</sup> order. The electrostatic interaction between MOF/ $\text{NH}_2/\text{Fe}_3\text{O}_4$  composite and MO dye could arise from the amino group and La(III) of the MOF with the functional groups of MO dye such as sulfonate, azo group, and aromatic ring. So, the functionalization of MOF/ $\text{NH}_2/\text{Fe}_3\text{O}_4$  composite with active adsorption sites was achieved powerfully.

**3.4. Thermodynamic Parameters of Adsorption.** For a better understanding of the behavior of MO dye adsorption on the surface of MOF/ $\text{NH}_2/\text{Fe}_3\text{O}_4$  composite, adsorption thermodynamic parameters were calculated. Moreover, the thermodynamic parameters help the determination of whether the adsorption process is spontaneous. The thermodynamic parameters include entropy change ( $\Delta S^0$ ), enthalpy change ( $\Delta H^0$ ), and Gibbs free-energy change ( $\Delta G^0$ ) and can be calculated using Eq.(7) and Eq.(8).

$$\Delta G^0 = -RT \ln K_0, \quad (7)$$

$$\ln K_0 = -\frac{\Delta H^0}{RT} + \frac{\Delta S^0}{R}, \quad (8)$$

where  $T$ ,  $R$ , and  $K_0$  denote the temperature (K), gas constant ( $8.314 \text{ J mol}^{-1}$ ), and distribution coefficient, respectively. The thermodynamic parameters of MO adsorption on the surface of MOF/ $\text{NH}_2/\text{Fe}_3\text{O}_4$  composite were calculated and tabulated in Table 2. The entropy change ( $\Delta S^0$ ) and enthalpy change ( $\Delta H^0$ ) of adsorption were calculated using Van't Hoff plot and their values were determined from the slope and intercept.

According to Table 2, the MO adsorption on MOF/ $\text{NH}_2/\text{Fe}_3\text{O}_4$  surface is a spontaneous process as the  $\Delta G^0$  values are negative [64, 65]. Moreover, the  $\Delta G^0$  values are in the range of 0 to  $-20.0 \text{ kJ mol}^{-1}$  that indicate the chemical adsorption of MO on the adsorbent surface. The positive value of entropy change ( $\Delta S^0$ ) is an indication of random motion resulting from the disorder during the adsorption process at the solid-liquid interface, while the positive value of enthalpy



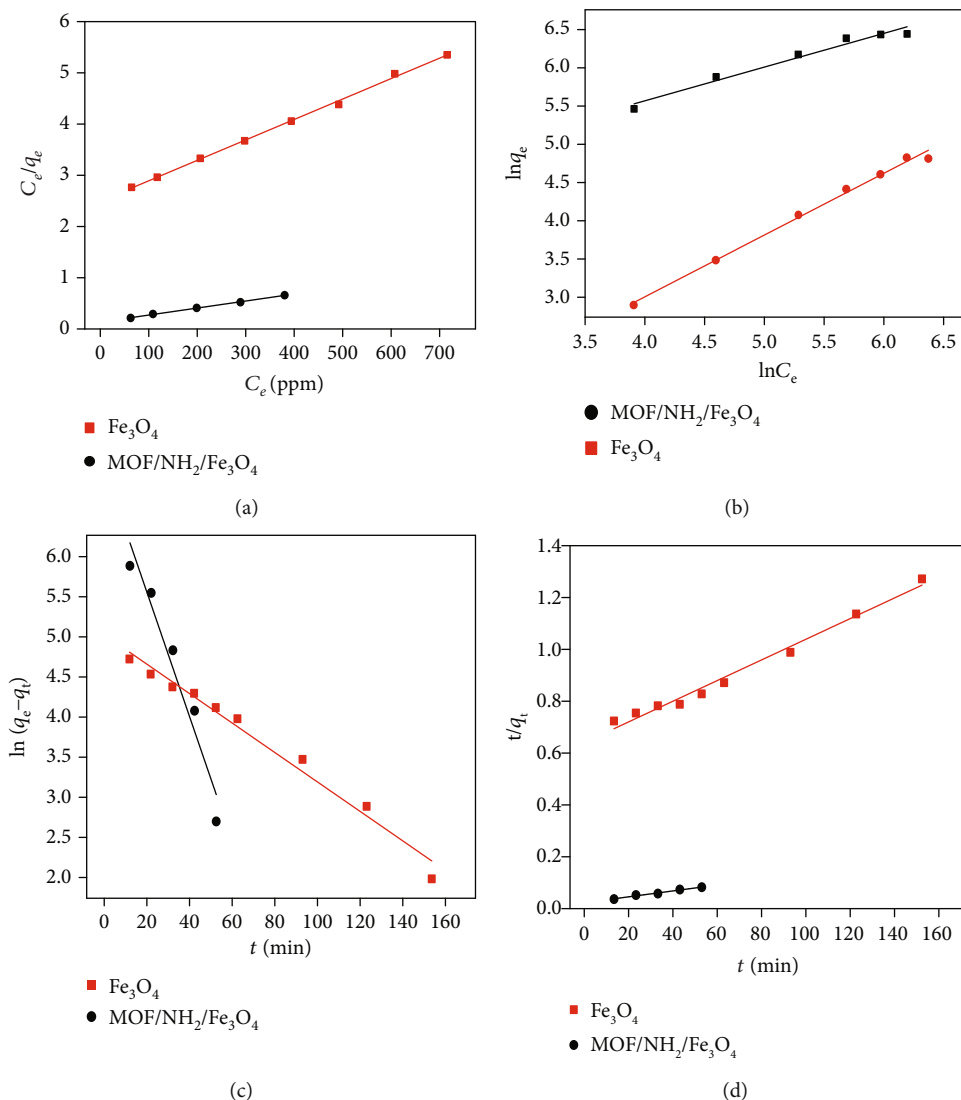


FIGURE 5: The fitting of adsorption data to the Langmuir model (a), the Freundlich model (b), pseudo 1<sup>st</sup> order (c), and pseudo 2<sup>nd</sup> order for the adsorption of MO dye on the surface of MOF/NH<sub>2</sub>/Fe<sub>3</sub>O<sub>4</sub> composite and Fe<sub>3</sub>O<sub>4</sub> nanoparticles.

TABLE 2: The thermodynamic parameters for the adsorption of MO on the surface of MOF/NH<sub>2</sub>/Fe<sub>3</sub>O<sub>4</sub> composite.

T (K)	$\ln K^0$	$\Delta S^0$ (J/mol/K)	$\Delta H^0$ (kJ/mol)	$\Delta G^0$ (kJ/mol)
298.15	4.8055			-11.905
308.15	5.4967	0.0362	1.73x10 <sup>-6</sup>	-14.075
318.15	5.7611			-15.231

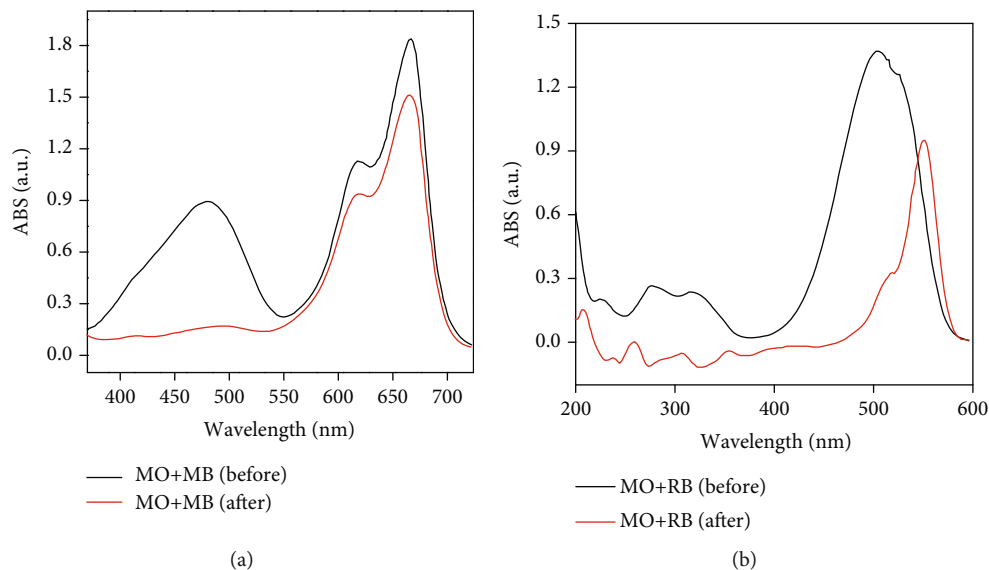
change ( $\Delta H^0$ ) is an indication of the endothermic behavior of MO adsorption on the surface of the MOF/NH<sub>2</sub>/Fe<sub>3</sub>O<sub>4</sub> composite. This means that the adsorption of MO on the MOF/NH<sub>2</sub>/Fe<sub>3</sub>O<sub>4</sub> surface is increased by increasing the temperature and this temperature will be consumed for the completeness of the adsorption reaction.

3.5. Comparative Study. For the assessment of adsorbent performance, the maximum adsorption capacity of MOF/

NH<sub>2</sub>/Fe<sub>3</sub>O<sub>4</sub> composite was compared with many commercial adsorbents of MO dye as tabulated in Table 3. According to Table 3, those previously reported adsorbents showed clearly lower adsorption capacities than MOF/NH<sub>2</sub>/Fe<sub>3</sub>O<sub>4</sub> composite. By comparing,  $q_m$  values of MOF/NH<sub>2</sub>/Fe<sub>3</sub>O<sub>4</sub> were many times more than other adsorbents. This enhanced adsorption capacity of MOF/NH<sub>2</sub>/Fe<sub>3</sub>O<sub>4</sub> composite may result from many reasons including the high surface area of the adsorbent, the presence of NH<sub>2</sub> on the surface of MOF that act as chelating arms to uptake the dye via electrostatic attraction, the intense +ve charge of La(III) of MOF that helps the strong electrostatic attraction between the anionic dye and adsorbent, and the host-guest interactions resulted from the embedding of dye within the pores of the MOF. Additionally, the presence of Fe<sub>3</sub>O<sub>4</sub> nanoparticles could effectively enhance the adsorption capacity of the composite due to its high surface area and adsorption power besides their role in magnetic separation to ease the reusability and reduce the treatment cost. Subsequently, this comparison

TABLE 3: Comparison the adsorption capacity of MOF/NH<sub>2</sub>/Fe<sub>3</sub>O<sub>4</sub> composite with previously reported adsorbents for the removal of MO dye.

Adsorbent	Removal capacity (mg/g)	Ref.
MOF/NH <sub>2</sub> /Fe <sub>3</sub> O <sub>4</sub>	618.0	This study
Cross-linked chitosan/-cyclodextrin composite	392.0	[66]
Ethylenediamine-grafted MIL-101	194.0	[67]
MIL-101 metal-organic frameworks	277.0	[68]
Chitosan/polyvinyl alcohol/zeolite electrospun composite	153.0	[69]
Mesoporous carbon	294.0	[70]
Chitosan/Al <sub>2</sub> O <sub>3</sub> /Fe <sub>3</sub> O <sub>4</sub>	416.0	[71]
Protonated cross-linked chitosan	180.0	[72]
Chitosan/clay/Fe <sub>3</sub> O <sub>4</sub>	149.0	[73]
Preyssler grafted magnetic chitosan	88.5	[74]
Chitosan/Kaolin/ $\gamma$ -Fe <sub>2</sub> O <sub>3</sub> nanocomposites	37.0	[75]
Y-Fe <sub>2</sub> O <sub>3</sub> /SiO <sub>2</sub> /chitosan composite	34.30	[76]

FIGURE 6: UV-vis absorption spectra of MO/MB (a) and MO/RB (b) before and after selective adsorption on the surface of MOF/NH<sub>2</sub>/Fe<sub>3</sub>O<sub>4</sub> composite.

can reveal that MOF/NH<sub>2</sub>/Fe<sub>3</sub>O<sub>4</sub> composite has brilliant efficiency for the adsorption of organic dyes from wastewater.

**3.6. Selective Adsorption.** The selective adsorption of MO by MOF/NH<sub>2</sub>/Fe<sub>3</sub>O<sub>4</sub> composite was performed using dye mixtures as shown in Figure 6. The mixtures of RB/MO and MB/MO were used to perform the selective adsorption study with dye initial concentrations of 10 mg/L for RB and MB dyes and 100 mg/L for MO dye, mixture volume of 50 mL, and an adsorbent dose of 20 mg. The solution was mixed for 30 minutes for adsorption followed by the collection of the adsorbent using an external magnetic field and the solution was examined for the presence of dyes. Then, the selective adsorption efficiency was calculated according to Eq.(9).

$$\text{Selective adsorption}(\%) = \frac{C_1}{C_1 + C_2} \times 100, \quad (9)$$

where  $C_1$  and  $C_2$  are representing the concentration of the mixture of two dyes after reaching the adsorption time.

According to Figure 6, MO dye was adsorbed selectively in the presence of RB and MB dyes on the surface of the MOF/NH<sub>2</sub>/Fe<sub>3</sub>O<sub>4</sub> composite.

UV-vis spectra of dye mixtures after adsorption showed the reduction of the MO dye band indicating selective adsorption. After adsorption, the selective adsorption efficiency of MO dye was 93% and 90% in the presence of MB and RB dyes, respectively. These results indicate the efficiency of the synthesized composite for the removal of MO from an aqueous solution. The results can be interpreted based on electrostatic attractions where the positively charged composite can adsorb the anionic dyes stronger than the cationic dyes.

**3.7. Desorption and Reusability Study.** A reusable adsorbent is cost-effective and in agreement with green chemistry

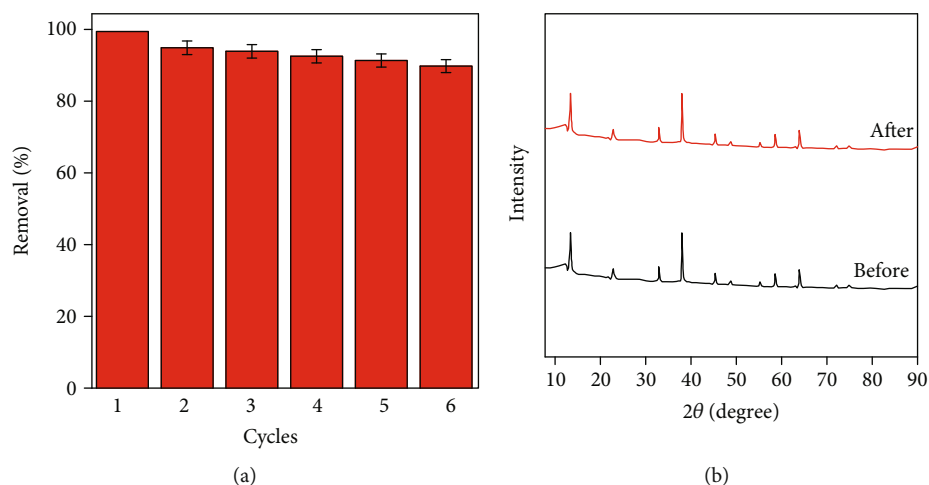


FIGURE 7: Reusability of MOF/NH<sub>2</sub>/Fe<sub>3</sub>O<sub>4</sub> composite for the removal of MO dye up to six cycles (a) and XRD pattern of MOF/NH<sub>2</sub>/Fe<sub>3</sub>O<sub>4</sub> composite before and after MO dye adsorption (b).

[77–79]. In this context, the reusability of MOF/NH<sub>2</sub>/Fe<sub>3</sub>O<sub>4</sub> composite was examined using methyl alcohol as an eluent for up to six successive cycles. The adsorption–desorption cycles were investigated six times as shown in Figure 7(a). During each cycle, the adsorbent was mixed with dye solution for adsorption. After that, the adsorbent was collected using an external magnet for desorption. The dye was desorbed from the surface of the adsorbent using methyl alcohol as eluent and the adsorbent was dried for usage in the next cycle. After each cycle, the solution was examined for the presence of dye, and the removal efficiency was calculated. According to Figure 7(a), the 1<sup>st</sup> cycle has the highest efficiency due to the presence of a large number of fresh adsorption sites. The next cycles showed a little drop in the removal efficiency due to the damage to nonrenewable adsorption sites. However, the last cycle showed that MOF/NH<sub>2</sub>/Fe<sub>3</sub>O<sub>4</sub> composite retained more than 90% of its efficiency. As can be shown in Figure 7(b), the composite's XRD after the sixth cycle of MO dye adsorption-desorption is identical to that obtained before dye adsorption, emphasizing the composite's stability during the reusability study. According to the reusability results, MOF/NH<sub>2</sub>/Fe<sub>3</sub>O<sub>4</sub> composite is considered a good regenerable adsorbent. The MOF/NH<sub>2</sub>/Fe<sub>3</sub>O<sub>4</sub> composite had advantages such as reusability at several stages without any change in the magnetic property, easy magnetic separation from aqueous solutions by the magnet, and fast pollutant adsorption.

#### 4. Conclusion

A reusable, highly efficient, and low-cost dye adsorbent, amino-functionalized MOF embedded with magnetic nanoparticles (MOF/NH<sub>2</sub>/Fe<sub>3</sub>O<sub>4</sub>) was well fabricated and the proper techniques were used for characterization. The synthetic approach involved the functionalization of porous MOF with amino groups to act as arms for dye capturing followed by the embedding of magnetic nanoparticles within MOF pores to increase its adsorption efficiency besides the

ease of collection with an external magnet. The lanthanum sites and the large surface area of the synthesized adsorbent could be responsible for the effective adsorption of MO dye from an aqueous solution with  $q_m$  of 618 mg/g which is higher than many reported adsorbents. The kinetics and isotherm studies indicated that the MO uptake on MOF/NH<sub>2</sub>/Fe<sub>3</sub>O<sub>4</sub> composite surface was achieved as a monolayer via a chemisorption mechanism in which the lanthanum ion played a key role besides the amino group arms. Additionally, MOF/NH<sub>2</sub>/Fe<sub>3</sub>O<sub>4</sub> composite showed selective adsorption toward MO dye from cationic/anionic dye mixtures which is related to the electrostatic attraction between anionic MO dye and positively charged surface of the composite. Also, the reusability study of MOF/NH<sub>2</sub>/Fe<sub>3</sub>O<sub>4</sub> composite toward MO adsorption was examined up to six successive cycles with excellent efficiency. As a result, MOF/NH<sub>2</sub>/Fe<sub>3</sub>O<sub>4</sub> composite showed excellent ability for effective applications in dye removal from aqueous solutions.

#### Data Availability

The research data used to support the findings of this study are included within the article.

#### Conflicts of Interest

The authors declare that they have no conflicts of interest.

#### Acknowledgments

The authors extend their appreciation to the Deanship of Scientific Research at King Khalid University for funding this work through the research group program under grant number RGP.2/57/43. Also, this research was funded by Princess Nourah bint Abdulrahman University Researchers Supporting Project number PNURSP2022R42, Princess Nourah bint Abdulrahman University, Riyadh, Saudi Arabia.

## References

- [1] A. M. Elgarahy, K. Z. Elwakeel, S. H. Mohammad, and G. A. Elshoubaky, "A critical review of biosorption of dyes, heavy metals and metalloids from wastewater as an efficient and green process," *Cleaner Engineering and Technology*, vol. 4, p. 100209, 2021.
- [2] V. Katheresan, J. Kannedo, and S. Y. Lau, "Efficiency of various recent wastewater dye removal methods: a review," *Journal of Environmental Chemical Engineering*, vol. 6, no. 4, pp. 4676–4697, 2018.
- [3] S. Velusamy, A. Roy, S. Sundaram, and T. Kumar Mallick, "A review on heavy metal ions and containing dyes removal through graphene oxide-based adsorption strategies for textile wastewater treatment," *The Chemical Record*, vol. 21, no. 7, pp. 1570–1610, 2021.
- [4] S. I. Siddiqui, B. Fatima, N. Tara, G. Rathi, and S. A. Chaudhry, "Recent advances in remediation of synthetic dyes from wastewaters using sustainable and low-cost adsorbents," in *The Impact and Prospects of Green Chemistry for Textile Technology, the Textile Institute Book Series*, S. I. Siddiqui, Ed., pp. 471–507, Woodhead Publishing, 2019.
- [5] E. Routoula and S. V. Patwardhan, "Degradation of anthraquinone dyes from effluents: a review focusing on enzymatic dye degradation with industrial potential," *Environmental Science & Technology*, vol. 54, no. 2, pp. 647–664, 2020.
- [6] M. Ismail, K. Akhtar, M. I. Khan et al., "Pollution, toxicity and carcinogenicity of organic dyes and their catalytic bio-remediation," *Current Pharmaceutical Design*, vol. 25, no. 34, pp. 3645–3663, 2019.
- [7] J. Joseph, R. C. Radhakrishnan, J. K. Johnson, S. P. Joy, and J. Thomas, "Ion-exchange mediated removal of cationic dye-stuffs from water using ammonium phosphomolybdate," *Materials Chemistry and Physics*, vol. 242, article 122488, 2020.
- [8] A. Ghaffar, L. Zhang, X. Zhu, and B. Chen, "Porous PVdF/GO nanofibrous membranes for selective separation and recycling of charged organic dyes from water," *Environmental Science & Technology*, vol. 52, no. 7, pp. 4265–4274, 2018.
- [9] N. Nasrollahi, S. Aber, V. Vatanpour, and N. M. Mahmoodi, "The effect of amine functionalization of CuO and ZnO nanoparticles used as additives on the morphology and the permeation properties of polyethersulfone ultrafiltration nanocomposite membranes," *Composites Part B: Engineering*, vol. 154, pp. 388–409, 2018.
- [10] N. S. Alsaiani, A. Amari, K. M. Katubi, F. M. Alzahrani, F. B. Rebah, and M. A. Tahaon, "The synthesis of magnetic nitrogen-doped graphene oxide nanocomposite for the removal of reactive orange 12 dye," *Adsorption Science & Technology*, vol. 2022, article 9417542, 14 pages, 2022.
- [11] A. Amari, N. Elboughdiri, D. Ghernaout et al., "Multifunctional crosslinked chitosan/nitrogen-doped graphene quantum dot for wastewater treatment," *Ain Shams Engineering Journal*, vol. 12, no. 4, pp. 4007–4014, 2021.
- [12] A. Chowdhury, A. A. Khan, S. Kumari, and S. Hussain, "Superadsorbent Ni–Co–S/SDS nanocomposites for ultrahigh removal of cationic, anionic organic dyes and toxic metal ions: kinetics, isotherm and adsorption mechanism," *ACS Sustainable Chemistry & Engineering*, vol. 7, no. 4, pp. 4165–4176, 2019.
- [13] L. H. T. Nguyen, H. T. T. Nguyen, B. Q. G. Le et al., "Micro-wave-assisted solvothermal synthesis of defective zirconium-organic framework as a recyclable nano-adsorbent with superior adsorption capacity for efficient removal of toxic organic dyes," *Colloid and Interface Science Communications*, vol. 46, p. 100511, 2022.
- [14] N. M. Mahmoodi, B. Hayati, H. Bahrami, and M. Arami, "Dye adsorption and desorption properties of *Mentha pulegium* in single and binary systems," *Journal of Applied Polymer Science*, vol. 122, no. 3, pp. 1489–1499, 2011.
- [15] N. M. Mahmoodi, F. Najafi, and A. Neshat, "Poly (amido-amine-co-acrylic acid) copolymer: synthesis, characterization and dye removal ability," *Industrial Crops and Products*, vol. 42, pp. 119–125, 2013.
- [16] N. M. Mahmoodi, A. Taghizadeh, M. Taghizadeh, and M. A. S. Baglou, "Surface modified montmorillonite with cationic surfactants: preparation, characterization, and dye adsorption from aqueous solution," *Journal of Environmental Chemical Engineering*, vol. 7, no. 4, p. 103243, 2019.
- [17] B. Hayati, N. M. Mahmoodi, and A. Maleki, "Dendrimer–titania nanocomposite: synthesis and dye-removal capacity," *Research on Chemical Intermediates*, vol. 41, no. 6, pp. 3743–3757, 2015.
- [18] B. Hayati, N. M. Mahmoodi, M. Arami, and F. Mazaheri, "Dye removal from colored textile wastewater by poly (propylene imine) dendrimer: operational parameters and isotherm studies," *Clean-Soil, Air, Water*, vol. 39, no. 7, pp. 673–679, 2011.
- [19] A. Almasian, M. E. Olya, and N. M. Mahmoodi, "Preparation and adsorption behavior of diethylenetriamine/polyacrylonitrile composite nanofibers for a direct dye removal," *Fibers and Polymers*, vol. 16, no. 9, pp. 1925–1934, 2015.
- [20] M. Liu, W. Yin, T. L. Zhao, Q. Z. Yao, S. Q. Fu, and G. T. Zhou, "High-efficient removal of organic dyes from model wastewater using Mg(OH)<sub>2</sub>-MnO<sub>2</sub> nanocomposite: synergistic effects of adsorption, precipitation, and photodegradation," *Separation and Purification Technology*, vol. 272, p. 118901, 2021.
- [21] N. C. Cinperi, E. Ozturk, N. O. Yigit, and M. Kitis, "Treatment of woolen textile wastewater using membrane bioreactor, nanofiltration and reverse osmosis for reuse in production processes," *Journal of Cleaner Production*, vol. 223, pp. 837–848, 2019.
- [22] I. A. Obiora-Okafo and O. D. Onukwuli, "Characterization and optimization of spectrophotometric colour removal from dye containing wastewater by Coagulation-Flocculation," *Polish Journal of Chemical Technology*, vol. 20, no. 4, pp. 49–59, 2018.
- [23] N. T. Hien, L. H. Nguyen, H. T. Van et al., "Heterogeneous catalyst ozonation of Direct Black 22 from aqueous solution in the presence of metal slags originating from industrial solid wastes," *Separation and Purification Technology*, vol. 233, p. 115961, 2020.
- [24] N. M. Mahmoodi, M. Bashiri, and S. J. Moeen, "Synthesis of nickel-zinc ferrite magnetic nanoparticle and dye degradation using photocatalytic ozonation," *Materials Research Bulletin*, vol. 47, no. 12, pp. 4403–4408, 2012.
- [25] I. Elaissaoui, H. Akrou, S. Grassini, D. Fulginiti, and L. Bousselmi, "Effect of coating method on the structure and properties of a novel PbO<sub>2</sub> anode for electrochemical oxidation of Amaranth dye," *Chemosphere*, vol. 217, pp. 26–34, 2019.
- [26] N. S. Alsaiani, A. Amari, K. M. Katubi et al., "The biocatalytic degradation of organic dyes using laccase immobilized magnetic nanoparticles," *Applied Sciences*, vol. 11, no. 17, p. 8216, 2021.

- [27] A. Amari, F. M. Alzahrani, N. S. Alsaiani, K. M. Katubi, F. B. Rebah, and M. A. Tahoan, "Magnetic metal organic framework immobilized laccase for wastewater decolorization," *PRO*, vol. 9, no. 5, p. 774, 2021.
- [28] N. M. Mahmoodi and M. H. Saffar-Dastgerdi, "Clean Laccase immobilized nanobiocatalysts (graphene oxide - zeolite nanocomposites): from production to detailed biocatalytic degradation of organic pollutant," *Applied Catalysis B: Environmental*, vol. 268, p. 118443, 2020.
- [29] S. Moosavi, C. W. Lai, S. Gan, G. Zamiri, O. Akbarzadeh Pivehzhani, and M. R. Johan, "Application of efficient magnetic particles and activated carbon for dye removal from wastewater," *ACS Omega*, vol. 5, no. 33, pp. 20684–20697, 2020.
- [30] R. Gusain, N. Kumar, and S. S. Ray, "Recent advances in carbon nanomaterial-based adsorbents for water purification," *Coordination Chemistry Reviews*, vol. 405, p. 213111, 2020.
- [31] H. Karimi-Maleh, M. Shafieizadeh, M. A. Taher et al., "The role of magnetite/graphene oxide nano-composite as a high-efficiency adsorbent for removal of phenazopyridine residues from water samples, an experimental/theoretical investigation," *Journal of Molecular Liquids*, vol. 298, p. 112040, 2020.
- [32] Z. Li, L. Sellaoui, D. Franco et al., "Adsorption of hazardous dyes on functionalized multiwalled carbon nanotubes in single and binary systems: experimental study and physicochemical interpretation of the adsorption mechanism," *Chemical Engineering Journal*, vol. 389, p. 124467, 2020.
- [33] N. M. Mahmoodi, "Synthesis of magnetic carbon nanotube and photocatalytic dye degradation ability," *Environmental Monitoring and Assessment*, vol. 186, no. 9, pp. 5595–5604, 2014.
- [34] P. Nuengmatcha, "Mercapto-functionalized magnetic graphene quantum dots as adsorbent for Cd<sup>2+</sup> removal from wastewater," *Environmental Processes*, vol. 8, no. 3, pp. 1289–1306, 2021.
- [35] M. N. F. Norrrahim, N. A. M. Kasim, V. F. Knight et al., "Nanocellulose: a bioadsorbent for chemical contaminant remediation," *RSC Advances*, vol. 11, no. 13, pp. 7347–7368, 2021.
- [36] X. Xie, X. Huang, W. Lin et al., "Selective adsorption of cationic dyes for stable metal-organic framework ZJU-48," *ACS Omega*, vol. 5, no. 23, pp. 13595–13600, 2020.
- [37] M. Oveisi, M. A. Asli, and N. M. Mahmoodi, "Carbon nanotube based metal-organic framework nanocomposites: synthesis and their photocatalytic activity for decolorization of colored wastewater," *Inorganica Chimica Acta*, vol. 487, pp. 169–176, 2019.
- [38] N. M. Mahmoodi, M. Oveisi, M. Bakhtiari et al., "Environmentally friendly ultrasound-assisted synthesis of magnetic zeolitic imidazolate framework - graphene oxide nanocomposites and pollutant removal from water," *Journal of Molecular Liquids*, vol. 282, pp. 115–130, 2019.
- [39] S. Yu, H. Pang, S. Huang et al., "Recent advances in metal-organic framework membranes for water treatment: a review," *Science of the Total Environment*, vol. 800, p. 149662, 2021.
- [40] R. B. Lin, S. Xiang, W. Zhou, and B. Chen, "Microporous metal-organic framework materials for gas separation," *Chem*, vol. 6, no. 2, pp. 337–363, 2020.
- [41] B. Li, H. M. Wen, Y. Yu et al., "Nanospace within metal-organic frameworks for gas storage and separation," *Materials Today Nano*, vol. 2, pp. 21–49, 2018.
- [42] X. Fang, B. Zong, and S. Mao, "Metal-organic framework-based sensors for environmental contaminant sensing," *Nano-Micro Letters*, vol. 10, no. 4, pp. 1–19, 2018.
- [43] M. Wang, L. Guo, and D. Cao, "Metal-organic framework as luminescence turn-on sensor for selective detection of metal ions: absorbance caused enhancement mechanism," *Sensors and Actuators B: Chemical*, vol. 256, pp. 839–845, 2018.
- [44] M. Sarker, S. Shin, and S. H. Jhung, "Synthesis and functionalization of porous Zr-diaminostilbenedicarboxylate metal-organic framework for storage and stable delivery of ibuprofen," *ACS Omega*, vol. 4, no. 6, pp. 9860–9867, 2019.
- [45] S. Abednatanzi, P. G. Derakhshandeh, H. Depauw et al., "Mixed-metal metal-organic frameworks," *Chemical Society Reviews*, vol. 48, no. 9, pp. 2535–2565, 2019.
- [46] A. Yan, X. Liu, G. Qiu et al., "A simple solvothermal synthesis and characterization of round-biscuit-like Fe<sub>3</sub>O<sub>4</sub> nanoparticles with adjustable sizes," *Solid State Communications*, vol. 144, no. 7–8, pp. 315–318, 2007.
- [47] S. Dong, L. Peng, W. Wei, and T. Huang, "Three MOF-templated carbon nanocomposites for potential platforms of enzyme immobilization with improved electrochemical performance," *ACS Applied Materials & Interfaces*, vol. 10, no. 17, pp. 14665–14672, 2018.
- [48] G. Asab, E. A. Zereffa, and T. Abdo Seghne, "Synthesis of silica-coated Fe<sub>3</sub>O<sub>4</sub> nanoparticles by microemulsion method: characterization and evaluation of antimicrobial activity," *International Journal of Biomaterials*, vol. 2020, Article ID 4783612, 11 pages, 2020.
- [49] R. Wo, Q. L. Li, C. Zhu et al., "Preparation and characterization of functionalized metal-organic frameworks with core/shell magnetic particles (Fe<sub>3</sub>O<sub>4</sub>@ SiO<sub>2</sub>@ MOFs) for removal of Congo red and methylene blue from water solution," *Journal of Chemical & Engineering Data*, vol. 64, no. 6, pp. 2455–2463, 2019.
- [50] H. Liu, L. Zhu, H. Ma et al., "Copper (II)-coated Fe<sub>3</sub>O<sub>4</sub> nanoparticles as an efficient enzyme mimic for colorimetric detection of hydrogen peroxide," *Microchimica Acta*, vol. 186, no. 8, pp. 1–9, 2019.
- [51] L. Zhu, L. Zong, X. Wu et al., "Shapeable fibrous aerogels of metal-organic-frameworks templated with nanocellulose for rapid and large-capacity adsorption," *ACS Nano*, vol. 12, no. 5, pp. 4462–4468, 2018.
- [52] B. Zhang, Y. Wu, and L. Cha, "Removal of methyl orange dye using activated biochar derived from pomelo peel wastes: performance, isotherm, and kinetic studies," *Journal of Dispersion Science and Technology*, vol. 41, 2020.
- [53] N. Wang, J. Chen, J. Wang, J. Feng, and W. Yan, "Removal of methylene blue by Polyaniline/TiO<sub>2</sub> hydrate: adsorption kinetic, isotherm and mechanism studies," *Powder Technology*, vol. 347, pp. 93–102, 2019.
- [54] M. Setoodehkhah and S. Momeni, "Water soluble schiff base functionalized Fe<sub>3</sub>O<sub>4</sub> magnetic nano-particles as a novel adsorbent for the removal of Pb (II) and Cu (II) metal ions from aqueous solutions," *Journal of Inorganic and Organometallic Polymers and Materials*, vol. 28, no. 3, pp. 1098–1106, 2018.
- [55] S. A. Abdel-Gawad and H. M. Abdel-Aziz, "Removal of ethinylestradiol by adsorption process from aqueous solutions using entrapped activated carbon in alginate biopolymer: isotherm and statistical studies," *Applied Water Science*, vol. 9, no. 4, pp. 1–8, 2019.

- [56] G. F. Abu-Alsoud, K. A. Hawboldt, and C. S. Bottaro, "Comparison of four adsorption isotherm models for characterizing molecular recognition of individual phenolic compounds in porous tailor-made molecularly imprinted polymer films," *ACS Applied Materials & Interfaces*, vol. 12, no. 10, pp. 11998–12009, 2020.
- [57] H. A. Ahsaine, M. Zbair, Z. Anfar, Y. Naciri, N. El Alem, and M. J. M. T. C. Ezahri, "Cationic dyes adsorption onto high surface area 'almond shell' activated carbon: kinetics, equilibrium isotherms and surface statistical modeling," *Materials Today Chemistry*, vol. 8, pp. 121–132, 2018.
- [58] M. F. Siddiqui, E. A. Khan, and T. Alam Khan, "Synthesis of MoO<sub>3</sub>/polypyrrole nanocomposite and its adsorptive properties toward cadmium (II) and nile blue from aqueous solution: equilibrium isotherm and kinetics modeling," *Environmental Progress & Sustainable Energy*, vol. 38, no. 6, article e13249, 2019.
- [59] A. Murugesan, M. Divakaran, P. Raveendran, A. B. Nitin Nikamant, and K. J. Thelly, "An eco-friendly porous poly (imide-ether) s for the efficient removal of methylene blue: adsorption kinetics, isotherm, thermodynamics and reuse performances," *Journal of Polymers and the Environment*, vol. 27, no. 5, pp. 1007–1024, 2019.
- [60] A. K. Tolkou, S. Trikalioti, O. Makrogianni et al., "Chromium (VI) removal from water by lanthanum hybrid modified activated carbon produced from coconut shells," *Nanomaterials*, vol. 12, no. 7, p. 1067, 2022.
- [61] X. Xu, P. Li, S. Yang et al., "The performance and mechanism of a Mg-Al double-layer oxide in chloride ion removal from an aqueous solution," *Nanomaterials*, vol. 12, no. 5, p. 846, 2022.
- [62] Q. Lian, F. Islam, Z. U. Ahmad et al., "Enhanced adsorption of resorcinol onto phosphate functionalized graphene oxide synthesized via Arbusov Reaction: a proposed mechanism of hydrogen bonding and  $\pi$ - $\pi$  interactions," *Chemosphere*, vol. 280, article 130730, 2021.
- [63] I. Maamoun, R. Eljamal, O. Falyouna, K. Bensaida, Y. Sugihara, and O. Eljamal, "Insights into kinetics, isotherms and thermodynamics of phosphorus sorption onto nanoscale zero-valent iron," *Journal of Molecular Liquids*, vol. 328, p. 115402, 2021.
- [64] E. A. Gomaa and M. A. Tahoona, "Ion association and solvation behavior of copper sulfate in binary aqueous-methanol mixtures at different temperatures," *Journal of Molecular Liquids*, vol. 214, pp. 19–23, 2016.
- [65] M. A. Tahoona, E. A. Gomaa, and M. H. A. Suleiman, "Aqueous micro-hydration of Na<sup>+</sup> (H<sub>2</sub>O)<sub>n=1-7</sub> clusters: DFT study," *Open Chemistry*, vol. 17, no. 1, pp. 260–269, 2019.
- [66] Y. Jiang, B. Liu, J. Xu et al., "Cross-linked chitosan/ $\beta$ -cyclodextrin composite for selective removal of methyl orange: adsorption performance and mechanism," *Carbohydrate Polymers*, vol. 182, pp. 106–114, 2018.
- [67] E. Haque, J. E. Lee, I. T. Jang et al., "Adsorptive removal of methyl orange from aqueous solution with metal-organic frameworks, porous chromium-benzenedicarboxylates," *Journal of Hazardous Materials*, vol. 181, no. 1–3, pp. 535–542, 2010.
- [68] T. Shen, J. Luo, S. Zhang, and X. Luo, "Hierarchically meso-structured MIL-101 metal-organic frameworks with different mineralizing agents for adsorptive removal of methyl orange and methylene blue from aqueous solution," *Journal of Environmental Chemical Engineering*, vol. 3, no. 2, pp. 1372–1383, 2015.
- [69] U. Habiba, T. A. Siddique, J. J. L. Lee, T. C. Joo, B. C. Ang, and A. M. Afif, "Adsorption study of methyl orange by chitosan/polyvinyl alcohol/zeolite electrospun composite nanofibrous membrane," *Carbohydrate Polymers*, vol. 191, pp. 79–85, 2018.
- [70] N. Mohammadi, H. Khani, V. K. Gupta, E. Amereh, and S. Agarwal, "Adsorption process of methyl orange dye onto mesoporous carbon material- kinetic and thermodynamic studies," *Journal of Colloid and Interface Science*, vol. 362, no. 2, pp. 457–462, 2011.
- [71] B. Tanhaei, A. Ayati, M. Lahtinen, B. M. Vaziri, and M. Sillanpää, "A magnetic mesoporous chitosan based core-shells biopolymer for anionic dye adsorption: kinetic and isothermal study and application of ANN," *Journal of Applied Polymer Science*, vol. 133, no. 22, p. 43466, 2016.
- [72] R. Huang, Q. Liu, J. Huo, and B. Yang, "Adsorption of methyl orange onto protonated cross-linked chitosan," *Arabian Journal of Chemistry*, vol. 10, no. 1, pp. 24–32, 2017.
- [73] D.-W. Cho, B.-H. Jeon, C.-M. Chon, F. W. Schwartz, Y. Jeong, and H. Song, "Magnetic chitosan composite for adsorption of cationic and anionic dyes in aqueous solution," *Journal of Industrial and Engineering Chemistry*, vol. 28, pp. 60–66, 2015.
- [74] B. Tanhaei, A. Ayati, F. F. Bamoharram, M. Lahtinen, and M. Sillanpää, "A novel magnetic Preyessler acid grafted chitosan nano adsorbent: synthesis, characterization and adsorption activity," *Journal of Chemical Technology and Biotechnology*, vol. 91, no. 5, pp. 1452–1460, 2016.
- [75] R. Jiang, H. Zhu, and Y. Fu, "Equilibrium and kinetic studies on adsorption of methyl orange from aqueous solution on chitosan/kaolin/ $\gamma$ -Fe<sub>2</sub>O<sub>3</sub> nanocomposite," in *International Conference on Remote Sensing, Env. Transport. Eng.*, vol. 24, pp. 7565–7568, 2011.
- [76] H. Y. Zhu, R. Jiang, Y.-Q. Fu, J.-H. Jiang, L. Xiao, and G.-M. Zeng, "Preparation, characterization and dye adsorption properties of  $\gamma$ -Fe<sub>2</sub>O<sub>3</sub>/SiO<sub>2</sub>/chitosan composite," *Applied Surface Science*, vol. 258, no. 4, pp. 1337–1344, 2011.
- [77] F. M. Alzahrani, N. S. Alsaiani, K. M. Katubi et al., "Magnetic nitrogen-doped porous carbon nanocomposite for Pb (II) adsorption from aqueous solution," *Molecules*, vol. 26, no. 16, p. 4809, 2021.
- [78] N. S. Alsaiani, K. M. Katubi, F. M. Alzahrani et al., "Synthesis, characterization and application of polypyrrole functionalized nanocellulose for the removal of Cr (VI) from aqueous solution," *Polymers*, vol. 13, no. 21, p. 3691, 2021.
- [79] S. M. Siddeeg, A. Amari, M. A. Tahoona, N. S. Alsaiani, and F. B. Rebah, "Removal of meloxicam, piroxicam and Cd<sup>2+</sup> by Fe<sub>3</sub>O<sub>4</sub>/SiO<sub>2</sub>/glycidyl methacrylate-S-SH nanocomposite loaded with laccase," *Alexandria Engineering Journal*, vol. 59, no. 2, pp. 905–914, 2020.